scientific reports

Check for updates

OPEN

# Morphological variations of the interatrial septum and potential implications in equine cardiology

Lara Ibrahim[1]✉, Ingrid Vernemmen[2], Eva Buschmann[2], Gunther van Loon[2] & Pieter Cornillie[1]

**The interatrial septum morphology, shaped by the septum primum and secundum fusion, results in the formation of the fossa ovalis (FO) and its limbus. Incomplete fusion can lead to a patent foramen ovale (PFO), while complete fusion may produce septal ridges and pouches (SPs), with SPs in humans linked to ischemic stroke and atrial arrhythmias. In horses, atrial tachycardia and fibrillation often originate near the FO. This study examines adult equine interatrial septum morphology to enhance understanding the region and guide electrophysiological interventions for equine cardiac arrhythmias. Post-mortem examinations of 62 adult equine hearts, assessed the interatrial septum morphology from both right and left sides, measuring the dimensions of the FO and the craniocaudal length, and dorsoventral height of the SPs. Histological analysis at selected septal locations evaluated the wall's thickness and composition. Significant morphological variations were observed, particularly the consistent presence of right-sided SP. The septum wall comprises three layers, with the central layer containing cardiomyocytes in varied orientations, interspersed with fibroadipose tissue, features potentially contributing to atrial arrhythmias. Understanding the equine interatrial septum morphology is important for optimizing transseptal puncture outcomes, by facilitating accurate intracardiac echocardiography interpretation, guiding precise puncture site selection and improving procedural safety and efficacy.**

**Keywords** Septal pouch, Ridge, Transeptal puncture, Fossa ovalis, Arrhythmia, Horse

The cardiac interatrial septum exhibits considerable variations in appearance across different species including humans, pigs, and sheep[1,2]. Its development involves fusion of the embryonic septum primum and septum secundum, resulting in the adult configuration seen from within the right atrium as the floor of the fossa ovalis (FO) and its limbus, respectively[3,4]. In some cases, the two walls do not fuse completely, resulting in communication between the atria, known as a patent foramen ovale (PFO)[3,4]. This typically occurs due to inadequate closure of the foramen ovale after birth and is often regarded as a normal anatomical variation of the interatrial septum with minimal clinical significance. It is important to distinguish a PFO from an ostium secundum atrial septal defect, as they fundamentally differ in their origins and implications. Unlike a PFO, which develops postnatally, an ostium secundum atrial septum defect is a congenital anomaly characterized by improper development of the septum primum, leading to a larger structural opening between the atria that can have serious clinical consequences if left untreated[5–7]. When fusion is complete, the endocardial surface of the interatrial septum may have a smooth or uneven appearance. A protruding septal ridge may also be present. Additionally, a fully closed wall can result in the presence of septal pouches (SPs), which are pocket-like formations that can vary in size and length. Septal pouches may be located on the right, left, or both sides of the septum, depending on the specific sites and extent of fusion between the septum primum and septum secundum at birth[5].

The presence of SPs has significant clinical implications in humans. For instance, a left-sided SP has been linked to ischemic stroke due to thrombus formation from stagnant blood flow[5]. Moreover, the interatrial wall, especially at the SPs have been implicated in the maintenance of atrial arrhythmias such as atrial tachycardia and atrial fibrillation by disrupting normal cardiac conduction patterns. This disruption, due to the complex orientation of myocardial fibers interrupted by fibroadipose tissue, may facilitate re-entrant circuits through

[1]Department of Morphology, Imaging, Orthopedics, Rehabilitation and Nutrition, Faculty of Veterinary Medicine, Ghent University, Ghent, Belgium. [2]Equine Cardioteam Ghent, Department of Internal Medicine, Reproduction and Population Medicine, Faculty of Veterinary Medicine, Ghent University, Ghent, Belgium. ✉email: Lara.ibrahim@ugent.be

multiple mechanisms[8,9]. Both adipocytes and fibroblasts introduce spatial obstacles that disrupt normal electrical wave propagation, leading to conduction blocks, especially at high stimulation frequencies[10,11]. Adipocytes, particularly in epicardial and intramyocardial fat, force zigzag conduction pathways, slowing conduction velocity and increasing conduction block likelihood, as seen in sheep models[12]. Moreover, fibroblasts influence cardiac conduction by establishing electrotonic loading and elevating the resting membrane potential of cardiomyocytes. This functional coupling prolongs the refractory period of the cardiomyocytes by slowing sodium channel recovery, thereby promoting the development of re-entry mechanisms in these areas in multiple species[13–15].

In equine medicine, atrial arrhythmias, particularly atrial fibrillation, present a challenge and may affect the performance and cardiovascular health of horses[16,17]. Minimally invasive cardiac techniques, such as transcatheter electrophysiological studies and three-dimensional electro-anatomical mapping, have been employed to determine the origin of these arrhythmias[18–22]. The origin of atrial tachycardia in the right atrium has been associated with the area of the myocardial sleeves caudal to the FO[20,23]. However, to further investigate the origin of atrial arrythmias in the left atrium, access to this heart chamber is critical. Catheterization of the left side of the heart typically required a more invasive approach via the carotid artery[19]. In this context, the transeptal puncture (TSP) procedure has emerged as a minimally invasive, valuable solution that provides access to the left atrium by puncturing the interatrial septum at the FO. Recent findings suggest that the pulmonary veins in horses are a potential source of atrial fibrillation[24,25], highlighting the potential of TSP for in-depth electrophysiological studies and ablation in the left atrium. Successful experimental TSP has been achieved in adult horses using both the transhepatic and jugular vein approaches[26,27]. The jugular vein approach was shown to be feasible to implement in catheter-based procedures and is currently being applied in clinical patients[26]. However, transient atrial arrhythmias, particularly atrial fibrillation, have been observed during the TSP procedure[26,27]. To advance the TSP technique, a comprehensive understanding of the FO morphology, thickness of the interatrial septum of the adult horse, and composition of the wall of the interatrial septum is needed.

A better understanding of the interatrial structures, including their inter-individual variations, wall composition, and thickness, might provide useful information for advancing intracardiac procedures such as TSP. Therefore, this study aimed to elucidate the morphological characteristics of the equine interatrial septum. First, the gross anatomical differences in the interatrial septum among horses were studied and compared to other species. Recognizing these gross anatomical variations among horses is important for future development of equine cardiology and cardiac interventions, as it allows for more accurate diagnosis and enhances the effectiveness of treatments for cardiac diseases in this species. Subsequently, the microscopic properties of the interatrial wall, with the aim of identifying any arrhythmogenic properties, were investigated. Finally, wall thickness was measured at different locations in the interatrial septum as this might help in selecting the puncture location for TSP.

## Materials and methods

### Study population

Post-mortem examinations were conducted on the hearts of 62 adult horses, comprising 11 obtained from an abattoir and 51 euthanized for non-cardiac reasons and donated by their owners for research purposes. Informed consent was obtained from the owners of the 51 horses. As these animals were euthanized for reasons unrelated to this study, specific details regarding their euthanasia protocols are unavailable. The specimens were collected over a period of 3 years, and this is study adhered to the ethical guidelines outlined by the Ethical Committee of the Faculty of Veterinary Medicine, Ghent University, Belgium. Clinical histories of the 51 euthanized horses showed limited ante-mortem cardiological evaluations, with 10 having normal transthoracic echocardiograms, 1 showing mild mitral valve regurgitation, and the rest lacking records of any cardiac examination. Exercise histories were unavailable for all horses. Among the 51 euthanized horses, the population consisted of 48 warmblood horses, 1 pony, 1 Friesian, and 1 trotter, comprising 23 mares and 28 stallions or geldings. The horses within the population were 13 ± 7 years old (mean ± standard deviation). Post-mortem measurements of body weight ranged between 282 and 700 kg, with an average weight of 513 ± 91 kg. Information regarding breed, sex, and weight were unavailable for 11 horses from the abattoir.

### Gross anatomy

Hearts were collected and examined post-mortem within 1 hour (33 horses), and for those examined beyond 1 hour (11 horses between 1 and 24 hours and 7 horses between 24 and 48 hours), the hearts kept in situ were stored in 4 °C to minimize post-mortem changes. To access the right atrium, an incision was made through the *sinus venarum cavarum (facies atrialis)*, cutting through the lateral wall of the cranial vena cava into the right atrium and further towards the lateral wall of the caudal vena cava (Fig. 1A). The left atrium was exposed by an incision starting from the caudal border of the left ventricle and extending dorsally through the left atrium and pulmonary veins. The surface of the interatrial septum on each atrial side was examined and categorized as either smooth or uneven. The absence of visible irregularities, creating a consistent, uninterrupted surface, defined smooth surfaces; conversely, surfaces displaying any depressions or irregularities were classified as uneven. The presence of a septal ridge, characterized by a distinct fold of protruding tissue on the interatrial septum, was recorded when observed. After macroscopic identification of the FO on the right side of the interatrial septum, measurements of the craniocaudal length and dorsoventral height were made caudal to the limbus (Fig. 1B). The presence of PFO or a SP in the interatrial septum was evaluated using a probe, noting whether it was a right-sided or left-sided SP. Measurements of craniocaudal length (distance between the opening at the level of the limbus and fundus of the SP) and dorsoventral height of the SP at its opening were measured using a caliper (Fig. 1B,C). The orientation of the fundus of the SP was also noted. Each measurement was performed three times, and the average (rounded to the nearest whole number) was recorded. Photographs of the specimens

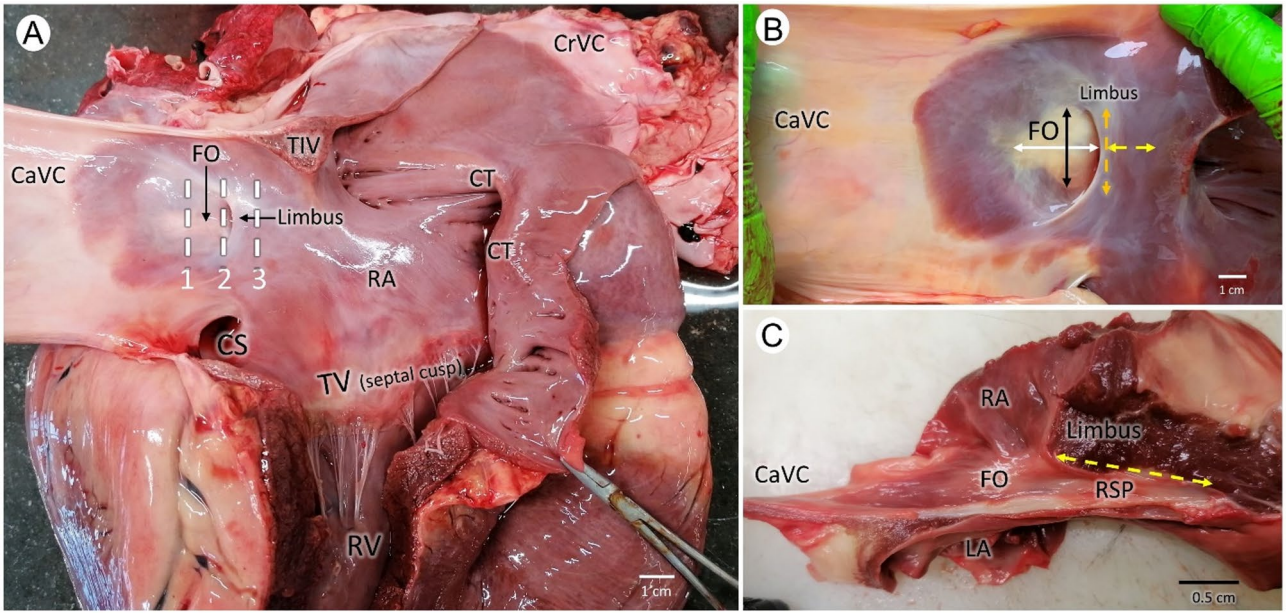


**Fig. 1**. Right atrial (RA) landmarks after lateral opening of the sinus venarum cavarum (facies atrialis) (A), right is cranial and top is dorsal. The locations of sample collection for histological evaluation are indicated with three dashed lines annotated as 1, 2 and 3 each corresponding to a specific level: level 1 (1) was located 1 cm caudal to the limbus, level 2 (2) was positioned at the entrance of the right-sided septal pouch (RSP), and level 3 (3) was taken at the RSP. B: Measurements of the fossa ovalis (FO) and RSP are shown. The FO craniocaudal length (white double-headed arrow) and dorsoventral height (black double-headed arrow) were measured caudally to the limbus. The RSP craniocaudal length (yellow double-headed arrow) and dorsoventral height (orange double-headed arrow) were also measured. Right is cranial and top is dorsal. C: After a cut on the craniocaudal axis, the FO and the RSP, covered by the limbus (cross-sectioned), are shown. Right is cranial and top is right. The length of the RSP is indicated by the yellow double-headed arrow. *CaVC* caudal vena cava, *CrVC* cranial vena cava, *CS* coronary sinus opening, *CT* crista terminalis, *RA* right atrium, *RV* right ventricle, *TIV* tuberculum intervenosum, *TV* tricuspid valve.

were captured with a 12MP digital camera under standard lighting conditions, and figures were created using Microsoft PowerPoint, Microsoft 365 (version 2502).

Morphological classifications of the interatrial septum, as per Holda et al., included several distinct categories: a smooth septum on both sides, devoid of PFO, septal ridges or SP; a PFO forming an interatrial channel; a left SP characterized by a pouch opening exclusively into the left atrial cavity; a right-sided SP featuring a pouch opening solely into the right atrial cavity; a double SP with two pouches, each opening into one atrium without interatrial connection; and a left-sided septal ridge with or without right-sided SP.

## Histology

Samples for histological analysis were collected from all hearts that could be collected within the first hour post-mortem to ensure fresh tissue was used ($n = 33$). A full-width rectangular sample, measuring 3 cm in dorsoventral height and 1 cm in craniocaudal length, was obtained from three distinct levels along the interatrial wall. Level 1 was located 1 cm caudal to the limbus, level 2 was positioned at the limbus, corresponding to the entrance of the right-sided SP, and level 3 was situated cranial to level 2, at the level of the right-sided SP when present (Fig. 1A). Following formalin fixation and paraffin embedding, slides of 8 µm thickness were stained using Masson's trichrome technique according to the protocol by IHC world[28]. Measurements were performed at the three positions sampled from the interatrial septum. First, three points on the right endocardial surface were selected, spaced 3 mm apart. Subsequently, the full thickness of the interatrial septum and muscle layer thickness were measured at these locations. Considering that the interatrial wall consists of two layers of fibrous connective tissue surrounding a central muscle layer, the thickness of the connective tissue was determined by subtracting the thickness of the muscle layer from the total thickness of the interatrial septum. This measurement reflects the combined thickness of the fibrous layers that encase the muscle.

## Statistical analysis

Normality of the descriptive variables was evaluated by examining histograms and quantile-quantile (Q-Q) plots. All data demonstrated normal distribution and are reported as means ± standard deviation. Chi-square/Fisher's exact tests were used to assess the association between the presence of a left-sided SP and a ridge with the left endocardial surface characteristics (smooth/uneven). Independent samples t-tests were used to compare mean depths and widths of the right-sided SP, left-sided SP, FO dimensions, and interatrial wall full thickness at the three chosen levels between male and female groups. Pearson's correlation analysis was conducted to

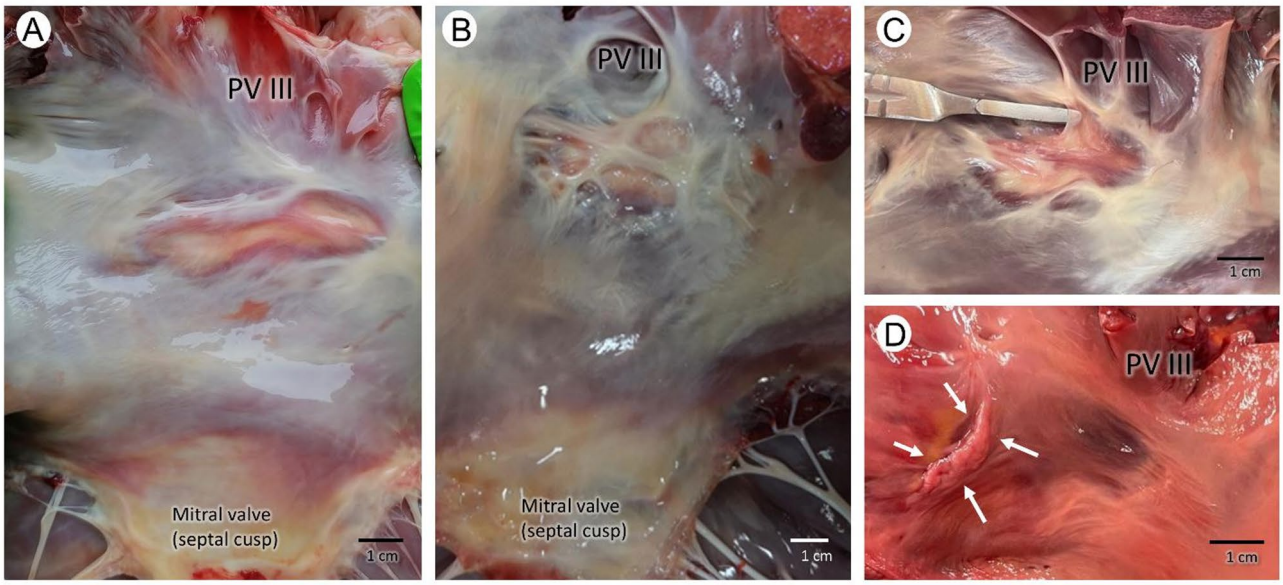


**Fig. 2**. A left-sided view on the interatrial septum shows macroscopic variations between horses. (**A**) Smooth endocardial surface, seen in the majority of horses; (**B**) uneven surface; **(C)** left-sided septal pouch, indicated with a scalpel holder inside it; and (**D**) a septal ridge, indicated by the white arrows. Right is caudal and top is dorsal. PV III, ostium III of the pulmonary veins.

| | RSP | LSP | DSP | RSP & LS ridge | DSP & LS ridge | Total number of horses (% of horses) |
|---|---|---|---|---|---|---|
| Smooth left surface | 26 (42%) | 0 | 9 (15%) | 2 (3%) | 2 (3%) | 39 (63%) |
| Uneven left surface | 16 (26%) | 0 | 7 (11%) | 0 | 0 | 23 (37%) |
| Total number of horses (% of horses) | 42 (68%) | 0 | 16 (26%) | 2 (3%) | 2 (3%) | 62 (100%) |

**Table 1**. Variations of the interatrial septum in adult horses: occurrence of a right-side septal pouch (RSP), left-sided septal pouch (LSP), double septal pouch (DSP) and a left-sided (LS) septal ridge, alongside the characterization of the left interatrial surface as smooth or uneven. The data is presented as the number of horses in each category, along with the corresponding percentages.

examine linear relationships between age, septal pouch dimensions, fossa ovalis dimensions, and interatrial wall thicknesses. Assumptions for the chi-square tests were evaluated using expected cell counts. Cohen's d and Cramer's V were calculated to assess effect sizes. A significance level of $p < 0.05$ was used for all statistical tests. Statistical analyses were performed using SPSS (SPSS Statistics 25, IBM, Brussels, Belgium).

## Results

The surface of the left side of the interatrial septum was predominantly smooth in 39/62 (63%) horses (Fig. 2A) and uneven in 23/62 (37%) horses (Fig. 2B). A left-sided septal ridge was found in 4/62 (6%) horses (Fig. 2D), in which the remaining left atrial side of the septum appeared smooth. On the right side of the interatrial septum, the endocardial surface was smooth over the FO with a prominent limbus observed in all horses. The FO, caudal to the limbus, appeared oval with a craniocaudal length and dorsoventral height of 20.9 ± 4.4 mm (range: 12 to 33 mm) and 11.1 ± 5.1 mm (range: 4 to 26 mm), respectively.

Thorough macroscopic inspection of the atrial septum did not identify a PFO in any of the examined hearts. A right-sided SP was present in all horses, measuring 12.2 ± 5.5 mm height at its base (range: 4 to 45 mm) and was funnel-shaped, extending 19.9 ± 6.8 mm in cranial direction (range: 6 to 42 mm). A left-sided SP was observed in 18/62 (29%) horses, of which two hearts also featured a left-sided septal ridge (Fig. 2C). The left-sided SP was 8.9 ± 8.3 mm in height at its opening (range: 2 to 26 mm) and extended 6.1 ± 3.9 mm in the caudal direction (range: 2 to 15 mm). As a right-sided SP was always present, all cases with a left-sided SP had a double SP.

The variations of the interatrial septum in adult horses, showing the occurrence of the right-sided SP, left-sided SP, double SP and left-sided septal ridge, along with the characterization of the left interatrial surface as either smooth or uneven, are detailed in Table 1. Furthermore, the prevalence of morphological variations in the interatrial septum of equine compared to those of human, porcine, and ovine hearts is shown in Fig. 3, with data adapted from Holda et al. (2018)[1,2].

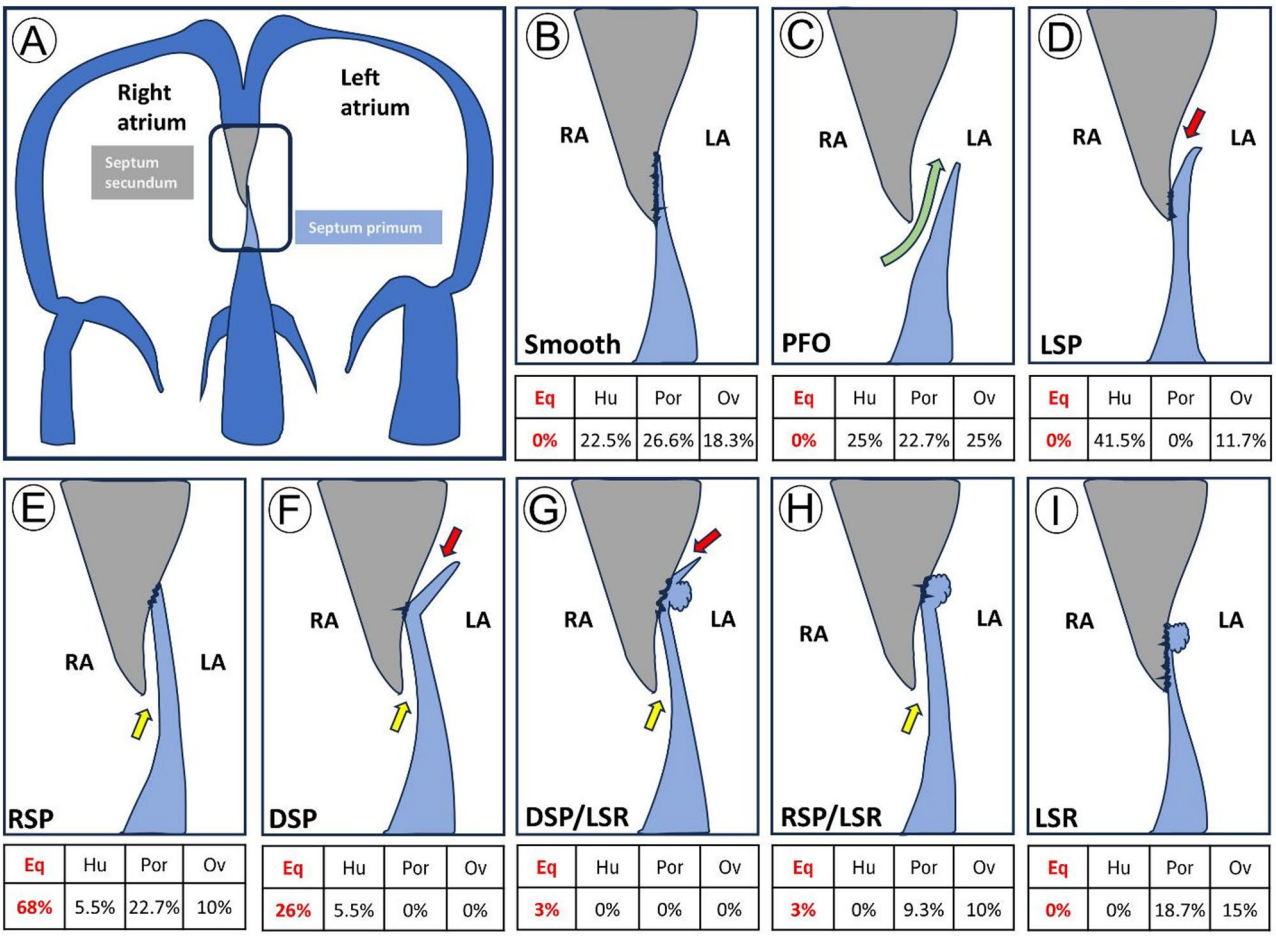


**Fig. 3**. Schematic overview of the interatrial septum in the heart. (**A**) General illustration of the interatrial septum formed by the fusion of the embryonic septum primum and secundum. (**B**–**I**) Different morphological presentations of the interatrial septum and their comparative prevalence among species: equine (Eq), human (Hu), porcine (Por), and ovine (Ov). (**B**) Smooth septum on both the right and left sides; (**C**) patent foramen ovale (PFO); (**D**) single left-sided septal pouch (LSP); (**E**) single right-sided septal pouch (RSP), the most common presentation in horses; (**F**) double septal pouch (DSP); (**G**) Double sided septal pouch with the presence of a left-sided septal ridge (LSR); (**H**) right-sided septal pouch coexisting with a left-sided septal ridge; (**I**) left-sided septal ridge. LA, left atrium; RA, right atrium.Adapted from Holda et al., 2018[1,2].

Histologically, the interatrial septum at all three locations was composed of three distinct layers (Fig. 4). Two layers of fibrous connective tissue were observed, beneath the right and left endocardial surfaces. The middle layer featured cardiomyocytes arranged in an undulating (wave-like) pattern. These cells were predominantly aligned lengthwise in the craniocaudal direction (visible as cross sections under microscopic examination). However, some cardiomyocytes were observed to have transverse and diagonal orientations (seen in longitudinal and oblique cuts, respectively). Fibers oriented in different directions were frequently seen to be tightly intertwined. Cardiomyocytes were frequently surrounded and interspersed with fibroadipose tissue. These histological features were consistently observed across all the three levels examined along the interatrial septum. The left-sided septal ridge exhibited a significant amount of adipose tissue surrounding the myocardial cells oriented in various directions (Fig. 5). Table 2 displays the measurements of interatrial wall thickness, muscle layer thickness, and proportion of connective tissue layers relative to the total wall thickness at the three examined locations.

Chi-square/Fisher's exact tests showed no significant association between the presence of a left-sided SP or a ridge and the smooth or uneven left endocardial surface. Independent samples t-tests ($N = 27$) revealed that males had a significantly thicker interatrial wall under the limbus (level 3) compared to females ($p = 0.003$), but no significant sex differences were found for other measurements. Pearson's correlation showed a positive correlation between right-sided SP depth and width ($N = 62$, $r = 0.520$, $p < 0.001$), and between the right-sided septal pouch width and fossa ovalis dorsoventral length ($N = 62$, $r = 0.418$, $p = 0.002$). Age correlated negatively with interatrial wall thickness at all three levels (r values ranging from −0.540 to −0.517, p values ranging from 0.011 to 0.012), while the thickness measurements at the three levels were positively correlated with each other (r values ranging from 0.458 to 0.872, all $p < 0.011$).

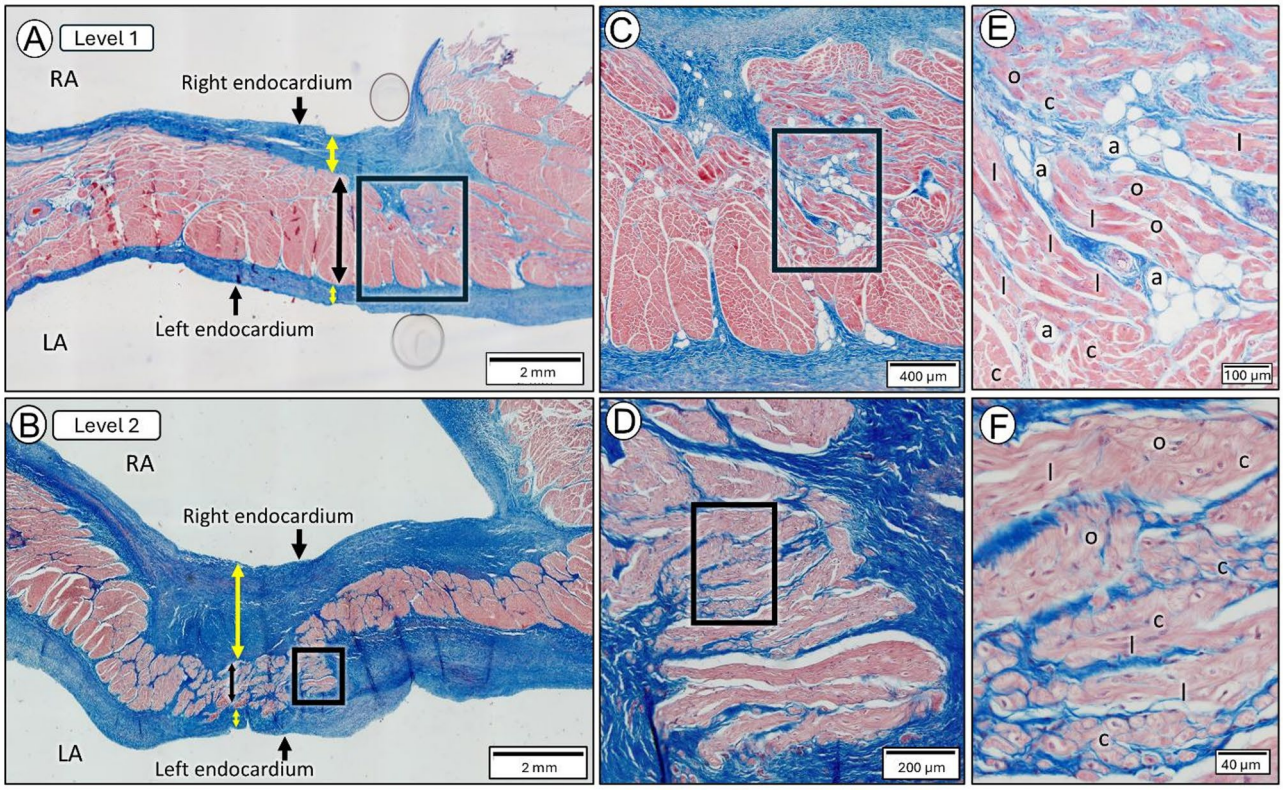


**Fig. 4**. Histological sections of the interatrial septum using Masson's trichrome staining at levels 1 and 2, as shown in Fig. 1A. Right is dorsal, and top is towards the right atrium. (**A**) Level 1, located 1 cm caudal to the limbus, illustrates the layered structure of the interatrial septum, featuring two subendocardial fibrous layers (yellow double arrows), with a myocardial layer (black double arrow) between them. (**B**) Level 2, positioned at the entrance of the right-sided septal pouch, exhibits a similar structural organization, with clearly defined fibrous (yellow double arrows) and myocardial (black double arrow) layers. In (**A**) and (**B**), the black boxes indicate the area for (**C**) and (**D**), respectively. (**C**,**D**) Magnified view of the myocardial layer at levels 1 and 2, revealing an undulating (wave-like) arrangement of myocardial fibers. In (**C**) and (**D**), the black boxes indicate the area for (**E**) and (**F**), respectively. (**E**–**F**) A detailed view of the myocardial fibers at Level 1 and Level 2 is shown in longitudinal cut (l) (showing transverse orientation), cross-section (c) (with fibers oriented in a craniocaudal direction), and oblique cut (o) (with fibers oriented obliquely within the interatrial septum). Adipose tissue (a) was observed interspersed between the cells in level 1. LA, left atrium; RA, right atrium.

## Discussion

The equine interatrial septum presents different morphological variations, primarily featuring a smooth left atrial septum, right-sided SP, and a prominent limbus. Remarkable variations were observed in the depth of the right atrial SP and the morphology of the left atrial surface, with and without SPs and septal ridges. These differences may be attributed to the theory of lifelong remodeling of the interatrial septum described in humans. According to this theory, constant friction between the flap valve (embryonic primary septum) and the surrounding interatrial septum causes microinjuries, leading to scar formation and eventual closure of the foramen ovale channel after birth. When the foramen ovale has a short flap valve, fusion is believed to typically occur early in life, resulting in a smooth septum. However, in cases where the flap valve is longer, fusion may occur at different levels (cranial, central, or caudal), resulting in the formation of a right-sided SP, a double SP, or a single left-sided SP[5]. Furthermore, similar to observations in humans, significant deposition of subendocardial connective tissue in the interatrial wall at the level of the right-sided SP in horses supports the hypothesis of flap valve fusion and subsequent SP formation. In this context, the health status of foals during the early neonatal period may influence the remodeling process of the interatrial septum. Weak foals with respiratory complications can develop right-sided hypertension, which may affect the timing and location of the closure of the foramen ovale over the septum primum and secundum. Persistent pulmonary hypertension in newborn foals often arises from difficulties in adapting to extrauterine life, leading to the maintenance of fetal circulation accompanied by right-to-left shunting through the PFO and ductus arteriosus under hypoxia conditions[7].

The prevalence of morphological features in the interatrial septum in horses differs notably from those observed in humans, pigs, and sheep. In contrast to these species, where a smooth septum, a PFO, and a single left-sided SP without a right-sided counterpart are common, none of these interatrial septum presentations were found in equine hearts in this study. The occurrence of PFO in adult horses is uncommon, although one case has been previously reported in a living adult horse[29]. All examined equine hearts had a right-sided SP, and

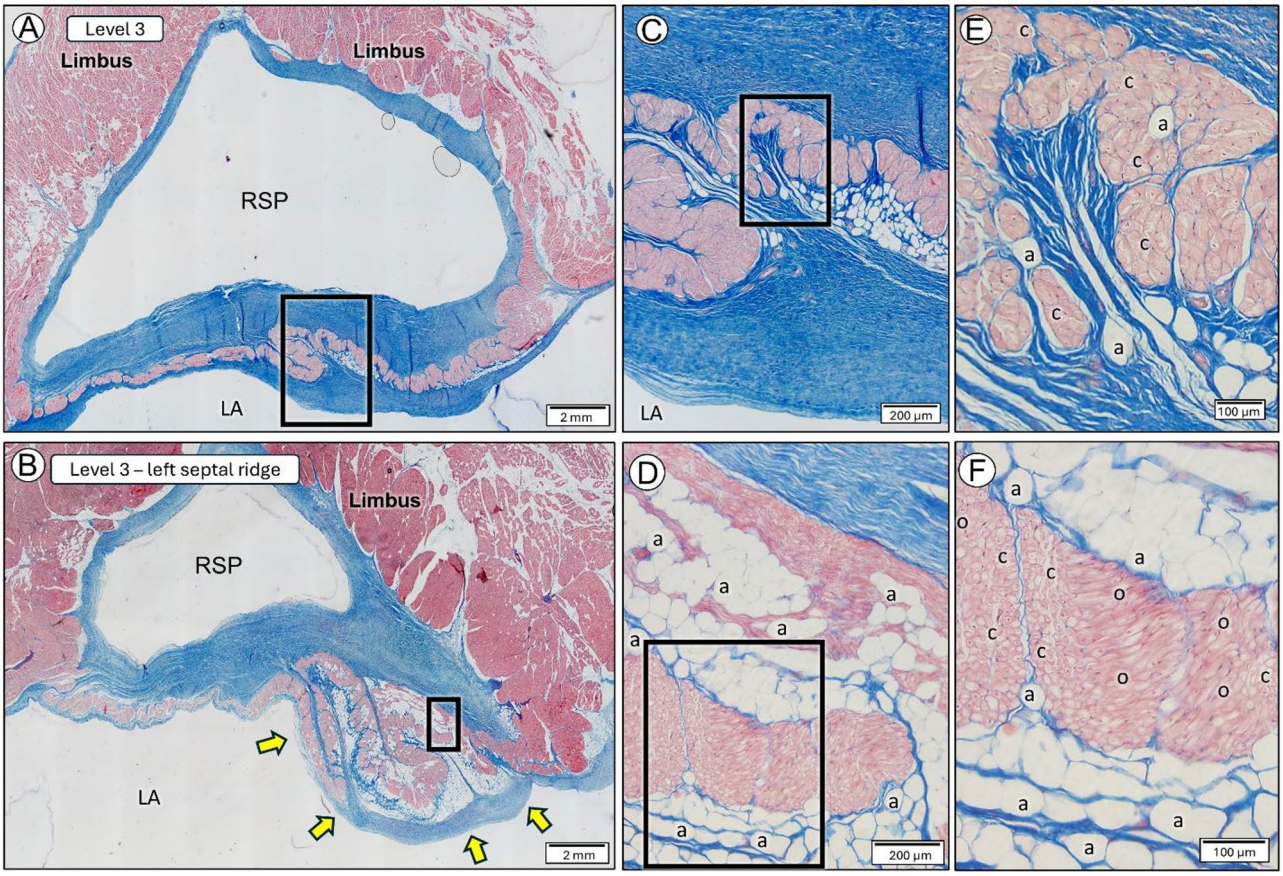


**Fig. 5**. Histological sections of the interatrial septum using Masson's trichrome staining at level 3, as shown in Fig. 1A. The right side is dorsal, and the top is oriented towards the right atrium. (**A**,**B**) Level 3, located at the right-sided septal pouch (RSP), shows the RSP in a cross section bordered by the limbus and interatrial septum. (**A**) Distinct undulating pattern of myocardial tissue is observed. The black box indicates the area magnified in (**C**). (**B**) A left-sided septal ridge is present (yellow arrows), with the black box indicating the area magnified in (**D**). (**C**) Magnified view of the myocardial layer from (**A**) showing a significant amount of adipose tissue (a). (**D**) A close-up of the left-sided septal ridge reveals a large amount of adipose tissue around and between the myocardial fibers. In (**C**) and (**D**), the black boxes indicate the area for (**E**) and (**F**), respectively. (**E**) A detailed view of the myocardial fibers in (**C**) shows them in cross-section (c), oriented in the craniocaudal direction, which is the most common orientation. (**F**) A detailed view of the myocardial fibers from (**D**) highlights the intertwining of fibers in cross-section (c) (craniocaudal direction) and fibers in oblique cut (o) (oblique orientation within the interatrial septum). An abundance of adipose tissue was also observed. LA, left atrium.

| | | | Connective tissue layer | |
|---|---|---|---|---|
| | Interatrial wall full thickness (mm) | Muscle layer thickness (mm) | Thickness (mm) | % to full thickness |
| Level 1: 1 cm caudal to the limbus | 4.0 ± 1.2 | 1.8 ± 0.7 | 2.1 ± 0.8 | 53% |
| Level 2: at the limbus/opening of the right-sided septal pouch | 3.7 ± 1.3 | 1.0 ± 0.4 | 2.6 ± 1.1 | 71% |
| Level 3: at the right-sided septal pouch | 3.7 ± 1.4 | 0.8 ± 0.5 | 2.9 ± 1.2 | 78% |

**Table 2**. Mean ± standard deviation of the interatrial wall thickness measurements obtained histologically in 33 horses at three specific locations: level 1 (1 cm caudal to the limbus), level 2 (at the limbus/opening of the right-sided septal pouch), and level 3 (at the right-sided septal pouch). Measurements comprised the thickness of the interatrial wall (mm), muscle layer thickness (mm), and connective tissue thickness, which were reported as both absolute values (mm) and percentage of full thickness.

simultaneously a left-sided SP in the minority of cases (29%), indicating a double SP configuration. In contrast, a right-sided SP is rare in humans (5.5%), and was found only in conjunction with a left-sided SP. Ovine hearts did not present a right-sided and left-sided SP simultaneously, whereas porcine hearts completely lacked a left-sided SP. The right-sided SP is consistently larger than the left-sided SP in horses, whereas the opposite has been

documented in humans[5]. The distinct interatrial septal morphology observed in horses, likely stems from a complex interplay of developmental and hemodynamic factors. Unlike the defined secondary foramen typical in humans, pigs and sheep, the equine septum primum develops into an elongated, perforated 'tunnel'[30]. This difference may originate from developmental variations in vena cavae and pulmonary vein positioning, which, in horses, resembles more closely the development in swine, and may impact septum formation. Postnatally, unique hemodynamic forces, shaped by the equine unguligrade posture and laterally compressed thorax, which likely result in altered blood flow patterns and pressure distributions within the right atrium compared to the orthograde humans and the more dorsoventrally compressed pigs and sheep, likely further influence septal morphology, affecting septal pouch formation[1].

Although the clinical significance of SPs remains unclear, a left-sided SP in humans is often associated with blood stasis, which can lead to thrombus formation and occult ischemic stroke[4,5,31–35]. However, the prevalence of a left-sided SP was higher in autopsied hearts compared to in vivo diagnosis using transesophageal ultrasound[36] or multi-slice computed tomography. This suggests that some left-sided SPs in humans may be hemodynamically inactive or that the sensitivity of the diagnostic techniques is too low[9]. Despite the large difference in heart size, the left-sided SP in horses was less deep (6.1 ± 3.9 mm) than that reported in humans (8.4 ± 5.1 mm deep), which might limit the risk for thrombus formation. The right-sided SP, which is usually longer, can accommodate larger volumes of blood. However, its potential association with blood stasis remains unclear and equine specific coagulation mechanisms might play a role. Additionally, whether the presence of muscular tissue within the wall of the pouch contributes to the removal of blood from the SP lumen remains to be determined. Furthermore, the consistent presence of a right-sided SP in horses, might influence right atrial pressure buffering, particularly during exercise, and potentially impact cardiac output. However, given the significant variability in pouch dimensions observed among horses, the magnitude of these functional effects is likely to vary considerably, emphasizing the need for further investigation to precisely quantify the impact of these anatomical variations on cardiac function.

A left-sided SP have been linked to a higher risk of atrial fibrillation in humans, potentially because of scar tissue formation resulting from gradual SP closure, which is believed to be proarrhythmogenic[9]. Similarly, the more elongated right-sided SP found in horses in this study may contribute to a higher prevalence of atrial fibrillation, as seen in humans with longer SPs, potentially due to the increase in atrial wall area and altered atrial conduction[37]. Horses often develop atrial arrhythmias such as atrial tachycardia and atrial fibrillation. In some cases, therapeutic intervention may be required using electro-anatomical mapping and radiofrequency catheter ablation to treat these conditions[16]. In cases of atrial tachycardia, 3D electro-anatomical mapping has identified local re-entry circuits often located in the medial wall of the caudal vena cava[19,21,22]. Myocardial sleeves from the caudal vena cava, caudally to the FO, and from the pulmonary veins exhibit morphological characteristics suggestive of their potential role in sustaining atrial tachycardia and atrial fibrillation[25,38]. This is similar to the involvement of myocardial sleeves in the pulmonary veins of humans in perpetuating atrial fibrillation[39–41]. Additionally, in human hearts, a connection of muscular bundles between myocardial sleeves in the pulmonary veins and the FO has been described, facilitating the propagation of electrical impulses originating from myocardial sleeves[8]. The interatrial septum at the FO and the right-sided SP in horses in this study showed a substantial presence of muscle tissue and morphological characteristics similar to those of the caudal vena cava. Factors such as complex myocardial fiber orientation and interruptions by fibroadipose tissue have been associated with delayed cardiac conduction and play a role in the pathogenesis of atrial fibrillation in humans and ovines[8,42]. These features suggest that the FO region may also serve as a substrate for atrial arrhythmias in horses. To determine how this region contributes to conduction abnormalities, connexin immunohistochemistry within the SP wall, similar to that performed in equine pulmonary veins[43], would reveal whether it actively participates in electrical impulse propagation or acts as a passive structure. Given the established link between connexin dysfunction and atrial fibrillation in humans, a high density of connexin 43 would suggest active conduction, while a sparse or disrupted distribution could indicate potential arrhythmogenic substrates[43–46].

The interatrial wall thickness showed and strong positive correlation between thickness measurements across the three levels as well as a statistically significant negative correlation with age, indicating potential age-dependent attenuation of the septum. Furthermore, the FO and SPs in the equine heart revealed a complex structure comprising a muscle tissue layer enclosed between two layers of connective tissue, along with the presence of adipose tissue, exhibiting similar layers and tissue composition as described in the human heart[8]. Notably, the thickness of the connective tissue was greater in the interatrial wall in the right-sided SP than at the entrance of the limbus or 1 cm caudal to the limbus. The data indicates that the percentage of connective tissue relative to the total wall thickness increases from caudal to cranial positions, reaching 78% in the right-sided SP. This variation in tissue composition may have implications for the TSP. The higher proportion of connective tissue, especially deeper in the right-sided SP, may present hurdles during TSP, making it more difficult to puncture compared to more muscular regions such as the interatrial wall at 1 cm caudal to the limbus. Transseptal puncture in the right-sided SP is currently avoided in horses as this would increase the risk for accidental aortic puncture and because it is more difficult to reach from a jugular vein approach[27]. The presence of myocardial tissue within the FO likely explains the induction of arrhythmias during TSP[26,27]. Furthermore, in contrast to the relatively thin interatrial septum observed in human patients and porcine models, the equine interatrial septum is considerably thicker, containing fibroadipose tissue which attenuates the transmural delivery of radiofrequency energy. Consequently, unintended perforation resulting from current ablation techniques used in horses is considered rather unlikely. Caution should be taken when ablating within a SP, as the reduced flow within the pouch may increase the likelihood of excessive heating, potentially resulting in steam pop or coagulum formation[47].

Although our study provides valuable insights into the morphological variations of the equine interatrial septum, there are several limitations to consider. The inclusion of predominantly warmblood horses in our study

sample limits the generalizability of our findings to other breeds. Moreover, although the euthanized horses were euthanized for non-cardiovascular reasons, comprehensive clinical histories, including ante-mortem cardiac evaluations and exercise records, were unavailable for the horses in this study. While this lack of detailed history could potentially obscure the influence of pre-existing cardiovascular conditions or physical activity on interatrial septal morphology, it is important to note that key cardiac conditions prevalent in humans, such as coronary artery disease and hypertension, are extremely rare in horses. Furthermore, we did not incorporate external body measurements, such as height at the withers or body length, to investigate potential correlations with the size and shape of atrial structures, although body weight was recorded. In addition, the use of post-mortem hearts may introduce artifacts that are not present in live animals, and histological analysis was limited to a subset of fresh hearts. The accuracy of histological measurements may also be compromised by tissue shrinkage during processing, which typically averages approximately 34%[48]. Therefore, the absolute thickness values reported in this study likely underestimate the actual dimensions of the interatrial wall. The shrinkage of the muscle is also considered to be greater than that of the connective tissue, which influences the proportion of connective tissue occupied compared with the full thickness. Moreover, our study focused exclusively on morphological characteristics; therefore, correlations between in vivo interventional and electrophysiological aspects were not explored. Future studies incorporating echocardiographic imaging, particularly 3D and intracardiac echocardiography, as well as electrophysiological mapping would help correlate morphological findings with functional properties and the clinical implications of interatrial septal variations, particularly concerning procedural planning, and role in arrhythmogenesis, ultimately leading to better outcomes.

Atrial SPs and septal ridges are natural anatomical variations of the interatrial septum. Understanding these structural nuances, as revealed by this study, may potentially enhance intracardiac echocardiographic interpretation during equine TSP. This could lead to more precise puncture site selection by allowing clinicians to avoid thicker or ridge areas, facilitating procedural planning, and potentially justify pre-operative TSP in predicted challenging cases, improving overall efficiency. Furthermore, anatomical knowledge of this area is important for the interpretation of ultrasound images when assessing the potential presence of PFO.

## Conclusion

Our study highlights the significant differences in equine interatrial septum morphology compared to other species, such as humans, pigs, and sheep, alongside clear variations within the equine population, particularly with a high prevalence of right-sided SP with a prominent limbus. Although the clinical significance of SPs in horses remains unclear, histological features with proarrhythmogenic properties have been found within the interatrial wall of the FO and SPs, suggesting the potential contribution of these structures to atrial arrhythmias. Overall, understanding equine interatrial septum morphology is important for accurate imaging assessment and decision making during minimally invasive cardiac procedures particularly TSP, where precise identification of septal pouch locations, dimensions, and ridges via intracardiac echocardiography would allow clinicians to select optimal puncture sites, minimizing complications and enhancing procedural safety and efficacy.

## Data availability

Data supporting the findings of this study are available from the corresponding author upon reasonable request.

Received: 3 January 2025; Accepted: 6 May 2025
Published online: 12 May 2025

## References

1. Holda, M. K., Holda, J., Koziej, M., Piatek, K. & Klimek-Piotrowska, W. Porcine heart interatrial septum anatomy. *Ann. Anat.* **217**, 24–28. https://doi.org/10.1016/j.aanat.2018.01.002 (2018).
2. Holda, M. K., Pietsch-Fulbiszewska, A., Trybus, M. & Koziej, M. Morphological variations of the interatrial septum in ovine heart. *PLoS One*. **13**, e0209604. https://doi.org/10.1371/journal.pone.0209604 (2018).
3. Anderson, R. H., Brown, N. A. & Webb, S. Development and structure of the atrial septum. *Heart* **88**, 104–110. https://doi.org/10.1136/heart.88.1.104 (2002).
4. Krishnan, S. C. & Salazar, M. Septal pouch in the left atrium: a new anatomical entity with potential for embolic complications. *JACC Cardiovasc. Interv.* **3**, 98–104. https://doi.org/10.1016/j.jcin.2009.07.017 (2010).
5. Holda, M. K. et al. Atrial septal pouch - Morphological features and clinical considerations. *Int. J. Cardiol.* **220**, 337–342. https://doi.org/10.1016/j.ijcard.2016.06.141 (2016).
6. Naqvi, N., McCarthy, K. P. & Ho, S. Y. Anatomy of the atrial septum and interatrial communications. *J. Thorac. Dis.* **10**, S2837–S2847. https://doi.org/10.21037/jtd.2018.02.18 (2018).
7. Schwarzwald, C. in *Equine Internal Medicine 4th ed.* 387–541 (2018).
8. Platonov, P. G., Mitrofanova, L., Ivanov, V. & Ho, S. Y. Substrates for intra-atrial and interatrial conduction in the atrial septum: anatomical study on 84 human hearts. *Heart Rhythm.* **5**, 1189–1195. https://doi.org/10.1016/j.hrthm.2008.04.025 (2008).
9. Holda, M. K. et al. Left atrial accessory appendages, diverticula, and left-sided septal pouch in multi-slice computed tomography. Association with atrial fibrillation and cerebrovascular accidents. *Int. J. Cardiol.* **244**, 163–168. https://doi.org/10.1016/j.ijcard.2017.06.042 (2017).
10. De Coster, T. et al. Arrhythmogenicity of fibro-fatty infiltrations. *Sci. Rep.* **8**, 2050. https://doi.org/10.1038/s41598-018-20450-w (2018).
11. Krishnan, A. et al. Are interactions between epicardial adipose tissue, cardiac fibroblasts and cardiac myocytes instrumental in atrial fibrosis and atrial fibrillation? *Cells* **10**, 2501 https://doi.org/10.3390/cells10092501 (2021).
12. Pouliopoulos, J. et al. Intramyocardial adiposity after myocardial infarction: new implications of a substrate for ventricular tachycardia. *Circulation* **128**, 2296–2308. https://doi.org/10.1161/CIRCULATIONAHA.113.002238 (2013).
13. Xie, Y. et al. Effects of fibroblast-myocyte coupling on cardiac conduction and vulnerability to reentry: A computational study. *Heart Rhythm.* **6**, 1641–1649. https://doi.org/10.1016/j.hrthm.2009.08.003 (2009).
14. Sachse, F. B., Moreno, A. P., Seemann, G. & Abildskov, J. A. A model of electrical conduction in cardiac tissue including fibroblasts. *Ann. Biomed. Eng.* **37**, 874–889. https://doi.org/10.1007/s10439-009-9667-4 (2009).

15. Simon-Chica, A., Wulfers, E. M. & Kohl, P. Nonmyocytes as electrophysiological contributors to cardiac excitation and conduction. *Am. J. Physiol. Heart Circ. Physiol.* **325**, H475–H491. https://doi.org/10.1152/ajpheart.00184.2023 (2023).
16. van Loon, G. Cardiac arrhythmias in horses. *Vet. Clin. North. Am. Eq Pract.* **35**, 85–102. https://doi.org/10.1016/j.cveq.2018.12.004 (2019).
17. Decloedt, A., Van Steenkiste, G., Vera, L., Buhl, R. & van Loon, G. Atrial fibrillation in horses part 1: pathophysiology. *Vet. J.* **263**, 105521. https://doi.org/10.1016/j.tvjl.2020.105521 (2020).
18. van Loon, G., Van Steenkiste, G., Vera, L. & Decloedt, A. Catheter-based electrical interventions to study, diagnose and treat arrhythmias in horses: from refractory period to electro-anatomical mapping. *Vet. J.* **263**, 105519. https://doi.org/10.1016/j.tvjl.2020.105519 (2020).
19. Van Steenkiste, G. et al. Three dimensional ultra-high-density electro-anatomical cardiac mapping in horses: methodology. *Equine Vet. J.* **52**, 765–772. https://doi.org/10.1111/evj.13229 (2020).
20. Van Steenkiste, G. et al. Detection of the origin of atrial tachycardia by 3D electro-anatomical mapping and treatment by radiofrequency catheter ablation in horses. *J. Vet. Intern. Med.* **36**, 1481–1490. https://doi.org/10.1111/jvim.16473 (2022).
21. Buschmann, E. et al. Successful caudal Vena Cava and pulmonary vein isolation in healthy horses using 3D electro-anatomical mapping and a contact force-guided ablation system. *Equine Vet. J.* https://doi.org/10.1111/evj.14037 (2023).
22. Buschmann, E. et al. Lesion size index-guided radiofrequency catheter ablation using an impedance-based three-dimensional mapping system to treat sustained atrial tachycardia in a horse. *Equine Vet. J.* https://doi.org/10.1111/evj.14424 (2024).
23. Buschmann, E. et al. Caudal Vena Cava isolation using ablation index-guided radiofrequency catheter ablation (CARTO 3) to treat sustained atrial tachycardia in horses. *J. Vet. Intern. Med.* https://doi.org/10.1111/jvim.17251 (2024).
24. Linz, D. et al. Pulmonary vein firing initiating atrial fibrillation in the horse: oversized dimensions but similar mechanisms. *J. Cardiovasc. Electrophysiol.* **31**, 1211–1212. https://doi.org/10.1111/jce.14422 (2020).
25. Kjeldsen, S. T. et al. Structural and electro-anatomical characterization of the equine pulmonary veins: implications for atrial fibrillation. *J. Vet. Cardiol.* **52**, 1–13. https://doi.org/10.1016/j.jvc.2024.01.001 (2024).
26. Vernemmen, I. et al. Intracardiac ultrasound-guided transseptal puncture in horses: outcome, follow-up, and perioperative anticoagulant treatment. *J. Vet. Intern. Med.* https://doi.org/10.1111/jvim.17158 (2024).
27. Vernemmen, I. et al. Development of an atrial transseptal puncture procedure in horses to access the left heart: an ultrasound-guided jugular vein and transhepatic approach. *Equine Vet. J.* https://doi.org/10.1111/evj.14084 (2024).
28. World, I. *Masson's trichrome staining protocol for collagen fibers*, (2024). https://ihcworld.com/2024/01/26/massons-trichrome-staining-protocol-for-collagen-fibers/
29. Vernemmen, I., Paulussen, E., Dauvillier, J., Decloedt, A. & van Loon, G. Three-dimensional and catheter-based intracardiac echocardiographic characterization of the interatrial septum in 2 horses with suspicion of a patent foramen ovale. *J. Vet. Intern. Med.* **36**, 1535–1542. https://doi.org/10.1111/jvim.16451 (2022).
30. Jensen, B., Wang, T. & Moorman, A. F. M. Evolution and development of the atrial septum. *Anat. Rec (Hoboken).* **302**, 32–48. https://doi.org/10.1002/ar.23914 (2019).
31. Abed, H. S. et al. Obesity results in progressive atrial structural and electrical remodeling: implications for atrial fibrillation. *Heart Rhythm.* **10**, 90–100. https://doi.org/10.1016/j.hrthm.2012.08.043 (2013).
32. Bandyopadhyay, S. & Mandana, K. Left atrial septal pouch: a potential source of systemic thromboembolism: incidental transesophageal echocardiogram findings. *Anesth. Analg.* **121**, 59–61. https://doi.org/10.1213/ANE.0000000000000684 (2015).
33. Aggarwal, S., Kalavakunta, J. & Gupta, V. Left atrial septal pouch thrombus: A common pathology in an uncommon location. *Int. J. Cardiol.* **212**, 369–370. https://doi.org/10.1016/j.ijcard.2016.03.046 (2016).
34. Sun, J. P. et al. Prevalence of atrial septal pouch and risk of ischemic stroke. *Int. J. Cardiol.* **214**, 37–40. https://doi.org/10.1016/j.ijcard.2016.03.119 (2016).
35. Wong, J. M. & Fisher, M. The potential role of the left atrial septal pouch in cryptogenic stroke. *Expert Rev. Cardiovasc. Ther.* **14**, 1–3. https://doi.org/10.1586/14779072.2015.1100536 (2016).
36. Wayangankar, S. A., Patel, J. H., Patel, B., Stavrakis, S. & Sivaram, C. A. Clinical and echocardiographic variables associated with LA septal pouch. *JACC Cardiovasc. Imaging.* **6**, 833–835. https://doi.org/10.1016/j.jcmg.2012.09.021 (2013).
37. Nair, M. et al. Chronic atrial fibrillation in patients with rheumatic heart disease: mapping and radiofrequency ablation of flutter circuits seen at initiation after cardioversion. *Circulation* **104**, 802–809. https://doi.org/10.1161/hc3201.094228 (2001).
38. Ibrahim, L., Buschmann, E., van Loon, G. & Cornillie, P. Morphological evidence of a potential arrhythmogenic substrate in the caudal and cranial Vena Cava in horses. *Equine Vet. J.* https://doi.org/10.1111/evj.14075 (2024).
39. Steiner, I., Hajkova, P., Kvasnicka, J. & Kholova, I. Myocardial sleeves of pulmonary veins and atrial fibrillation: a postmortem histopathological study of 100 subjects. *Virchows Arch.* **449**, 88–95. https://doi.org/10.1007/s00428-006-0197-2 (2006).
40. Szczepanek, E., Bolechala, F., Koziej, M., Jasinska, K. A. & Holda, M. K. Morphometric characteristics of myocardial sleeves of the pulmonary veins. *J. Cardiovasc. Electrophysiol.* **31**, 2455–2461. https://doi.org/10.1111/jce.14651 (2020).
41. Bredeloux, P., Pasqualin, C., Bordy, R., Maupoil, V. & Findlay, I. Automatic activity arising in cardiac muscle sleeves of the pulmonary vein. *Biomolecules.* https://doi.org/10.3390/biom12010023 (2021).
42. Samanta, R., Pouliopoulos, J., Thiagalingam, A. & Kovoor, P. Role of adipose tissue in the pathogenesis of cardiac arrhythmias. *Heart Rhythm.* **13**, 311–320. https://doi.org/10.1016/j.hrthm.2015.08.016 (2016).
43. Kovacs, S., Racz, B., Sotonyi, P. & Bakos, Z. Morphological and histological investigation of the conduction system in the equine atrial muscle sleeve of pulmonary veins. *Equine Vet. J.* **56**, 1059–1067. https://doi.org/10.1111/evj.13996 (2024).
44. Kato, T., Iwasaki, Y. K. & Nattel, S. Connexins and atrial fibrillation: filling in the gaps. *Circulation* **125**, 203–206. https://doi.org/10.1161/CIRCULATIONAHA.111.075432 (2012).
45. Poelzing, S. & Rosenbaum, D. S. Altered connexin43 expression produces arrhythmia substrate in heart failure. *Am. J. Physiol. Heart Circ. Physiol.* **287**, H1762–1770. https://doi.org/10.1152/ajpheart.00346.2004 (2004).
46. Jennings, M. M. & Donahue, J. K. Connexin remodeling contributes to atrial fibrillation. *J. Atr. Fibrillation.* **6**, 839. https://doi.org/10.4022/jafib.839 (2013).
47. Peng, L. Q. et al. Left atrial diverticula in patients referred for radiofrequency ablation of atrial fibrillation: assessment of prevalence and morphologic characteristics by dual-source computed tomography. *Circ. Arrhythm. Electrophysiol.* **5**, 345–350. https://doi.org/10.1161/CIRCEP.111.965665 (2012).
48. Paramasivan, S. et al. Evaluation of the Temporal relationship between formalin submersion time and routine tissue processing on resected head and neck specimen size. *Aust J. Otolaryngol.* **4**, 32–32. https://doi.org/10.21037/ajo-20-46 (2021).


## Acknowledgements

We wish to thank the owners who donated their horse for research which allowed us to perform this study. We would also like to thank Leen Claeys, Lorenzo Van Herrewege (Department of Pathobiology, Pharmacology and Zoological Medicine, Faculty of Veterinary Medicine, Ghent university) and Patrick Vervaet (Department of Morphology, Imaging, Orthopedics, Rehabilitation and Nutrition, Faculty of Veterinary Medicine, Ghent university) for help with data collection.

## Author contributions

LI contributed to designing and executing the study, analyzing and interpreting data, and drafting the manuscript. IV and EB assisted with study interpretation, as well as manuscript editing. GvL and PC contributed to study design, data analysis and interpretation, and manuscript revision. The final version of the manuscript was approved by all authors prior to submission.

## Declarations

## Competing interests

The authors declare no competing interests.

## Additional information

**Correspondence** and requests for materials should be addressed to L.I.

**Reprints and permissions information** is available at www.nature.com/reprints.

**Publisher's note** Springer Nature remains neutral with regard to jurisdictional claims in published maps and institutional affiliations.